4-Arylazo-3,5-diamino-1*H*-pyrazole CDK Inhibitors: SAR Study, Crystal Structure in Complex with CDK2, Selectivity, and Cellular Effects†

Vladimír Kryštof,‡ Petr Cankař,§ Iveta Fryšová,§ Jan Slouka,§ George Kontopidis,∥,⊥ Petr Džubák,# Marián Hajdúch,# Josef Srovnal,# Walter F. de Azevedo Jr.,⊗ Martin Orság,‡ Martina Paprskářová,‡ Jakub Rolčík,‡ Aleš Látr,‡ Peter M. Fischer,∥,○ and Miroslav Strnad*,‡

Laboratory of Growth Regulators, Faculty of Science, Palacký University and Institute of Experimental Botany, Šlechtitelů 11, 783 71 Olomouc, Czech Republic, Department of Organic Chemistry, Faculty of Science, Palacký University, tř. Svobody 8, 772 00 Olomouc, Czech Republic, Structure Based Design Group, Cyclacel Pharmaceuticals, Incorporated, James Lindsay Place, Dundee, DD1 5JJ, Scotland, United Kingdom, Laboratory of Experimental Medicine, Department of Pediatrics, Faculty of Medicine, Palacký University and Faculty Hospital, Puškinova 6, 775 20 Olomouc, Czech Republic, and Faculdade de Biociências, Pontifícia Universidade Católica do Rio Grande do Sul, Av. Ipiranga 6681, Porto Alegre, RS 90619-900, Brazil

Received May 15, 2006

In a routine screening of our small-molecule compound collection we recently identified 4-arylazo-3,5-diamino-1*H*-pyrazoles as a novel group of ATP antagonists with moderate potency against CDK2-cyclin E. A preliminary SAR study based on 35 analogues suggests ways in which the pharmacophore could be further optimized, for example, via substitutions in the 4-aryl ring. Enzyme kinetics studies with the lead compound and X-ray crystallography of an inhibitor−CDK2 complex demonstrated that its mode of inhibition is competitive. Functional kinase assays confirmed the selectivity toward CDKs, with a preference for CDK9-cyclin T1. The most potent inhibitor, 4-[(3,5-diamino-1*H*-pyrazol-4-yl)diazenyl]phenol **31b** (CAN508), reduced the frequency of S-phase cells of the cancer cell line HT-29 in antiproliferation assays. Further observed cellular effects included decreased phosphorylation of the retinoblastoma protein and the C-terminal domain of RNA polymerase II, inhibition of mRNA synthesis, and induction of the tumor suppressor protein p53, all of which are consistent with inhibition of CDK9.

Introduction

The cyclin-dependent kinases (CDKs[a]) are a family of serine/threonine protein kinases that play essential roles in the regulation of cell division. Individual CDKs phosphorylate distinct substrates in different phases of the cell cycle and are, therefore, classified as G1 (CDK4 and CDK6-D cyclins, CDK2-cyclin E), S (CDK2-cyclin A, CDK1-cyclin A), and G2/M (CDK1-cyclin B) phase-specific CDKs.[1,2] The activity of these kinases is tightly regulated at several levels: through interactions with negative and positive regulatory partners, activation by phosphorylation or dephosphorylation, and shifts in their subcellular localization. Cell cycle deregulation is frequently accompanied by altered CDK activity in many cancers, caused either by changed expression or activation of CDKs and/or their interacting proteins. For these reasons, cell cycle CDKs, especially CDK2 and CDK4, have been actively pursued as pharmacological targets for novel anticancer agents.[3−6]

During the past decade various drug discovery programs have led to the identification of many potent and selective ATP-antagonist inhibitors of CDKs, despite the fact that the active site in protein kinases is highly conserved (reviewed recently in refs 7−9). Generally, such inhibitors consist of structurally distinct, flat heterocyclic molecules, which enter the active site and compete with ATP, a feature usually demonstrated by enzyme kinetics and inhibitor-CDK2 cocrystal analyses. Anti-CDK drugs possess prominent inhibitory properties against cancer cells both in vitro and in vivo, and several are currently being evaluated in clinical trials as a new generation of anticancer chemotherapeutics.[10,11]

Apart from roles in cell cycle regulation, several CDKs also participate in other physiological processes such as neuronal functions (CDK5, CDK11), apoptosis (CDK1, CDK5), and transcription (CDK2, CDK7, CDK8, CDK9, CDK11); these processes have also been shown to be affected by pharmacological inhibitors of CDKs.[6,12] In particular, CDKs implicated in the regulation of transcription at the level of RNA polymerase II (RNAP-II) have recently attracted interest among medicinal chemists because of the roles of these CDKs during viral infection.[13,14] Small DNA viruses rely on host cell CDKs for their replication; some require the host expression apparatus, while others encode their own cyclins, which activate cellular CDKs or contain proteins that directly recruit CDKs to the nascent viral transcripts.[13] Some CDK inhibitors, such as flavopiridol and roscovitine, have already been shown to interfere with the replication of several viruses, and this activity is attributed to inhibition of transcription.[15−18]

These transcriptional CDK inhibitors may also have oncological applications. Until recently, the antiproliferative effects of CDK inhibitors (which are mainly oligospecific) against tumor cells were thought to be due to cellular attenuation of

* Corresponding author. Tel.: +420 585 634 850. Fax: +420 585 634 870. E-mail: strnad@aix.upol.cz.

† The structure has been deposited with the Protein Data Bank (PDB) under the accession code 2CLX.

‡ Palacký University and Institute of Experimental Botany.

§ Palacký University.

∥ Cyclacel Pharmaceuticals, Inc.

⊥ Current address: Veterinary Faculty, University of Thessaly, P. O. Box 199, 43100 Karditsa, Greece.

Palacký University and Faculty Hospital.

⊗ Pontifícia Universidade Católica do Rio Grande do Sul.

○ Current address: Centre for Biomolecular Sciences, School of Pharmacy, University of Nottingham, University Park, Nottingham NG7 2RD, U.K.

[a] Abbreviations: CDK, cyclin-dependent kinase; RNAP−II, RNA polymerase II; CTD, C-terminal domain; DRB, 5,6-dichloro-1-(*β*)-D-ribofuranosylbenzimidazole; BrdU, 5-bromo-2′-deoxyuridine; CEA, carcinoembryonic antigen; EpCAM, epithelial cell adhesion molecule; GAPDH, glyceraldehyde-3-phosphate dehydrogenase.

10.1021/jm0605740 CCC: $33.50
Published on Web 09/29/2006

CDK2 activity.[19] However, recent target validation studies have shown that CDK2 knockout mice are fully viable and, even, that cancer cells can proliferate in the absence of CDK2.[20,21] The exact reasons for the undoubted antitumor activity, both in vitro and in vivo, of many CDK inhibitors remain unclear, but probably more than one CDK must be targeted at the same time to achieve an antiproliferative effect. In particular, inhibition of the CDKs that mediate phosphorylation of the C-terminal domain (CTD) of RNAP-II is thought to contribute markedly to the cytotoxic potency of such compounds, as shown for instance with flavopiridol and roscovitine.[22−25] A rapid decline in levels of key proteins, due to inhibition of transcription, may be the ultimate cause of the cytoxicity of pharmacological inhibitors of CDKs, especially when both the affected protein and the corresponding mRNA have short half-lives. One such gene product is the antiapoptotic factor Mcl-1, which is crucial for the survival of a range of cell types. Its down-regulation either by roscovitine or siRNA is sufficient to induce apoptosis.[26,27] More particularly, selective CDK9 inhibition could serve as a potential therapeutic strategy against tumor invasion and metastasis, as recently demonstrated by the finding that inflammatory cytokine tumor necrosis factor-α promotes tumor progression through activation of matrix metalloproteinases.[28]

During the course of our ongoing CDK inhibitor discovery and development program, we have already identified several series of structurally diverse compounds that possess the ability to block CDK phosphorylating activities.[29−34] More recently, we discovered that the screening hit 4-phenylazo-3,5-diamino-1*H*-pyrazole compound **1b** inhibits CDK2-cyclin E. Although this inhibition is comparatively weak, the simple two-step synthetic assembly of the 4-phenylazo-3,5-diamino-1*H*-pyrazole system prompted us to develop a novel group of protein kinase inhibitors. We thus went on to synthesize a group of 35 3,5-diamino-1*H*-pyrazole derivatives substituted with different arylazo groups at position 4, to analyze their structure−activity relationships and to determine the in vitro antiproliferative properties of these compounds against cancer cell lines.

Chemistry

The 4-arylazo-3,5-diamino-1*H*-pyrazole CDK inhibitory compounds were synthesized as outlined in Scheme 1. The precursor hydrazones **a** were obtained by diazotization of the appropriate arylamines, followed by condensation with malonodinitrile. Finally, cyclocondensation of these dicyanohydrazones with hydrazine afforded the 4-arylazo-3,5-diamino-1*H*-pyrazoles **b**. In total, 12 hydrazones and 18 4-arylazo-3,5-diamino-1*H*-pyrazoles were synthesized for the first time. Reaction yields and compound characterization data are included in the Supporting Information, as well as relevant literature references for compounds already described (Supplementary Tables 1−3, Supporting Information).

Results and Discussion

CDK2 Kinase Inhibitory Activity. Routine screening of our compound libraries for protein kinase inhibitors led to the identification of **1b** as the first representative of a novel group of compounds that can diminish the catalytic activity of CDK2-cyclin E. In an effort to identify basic relationships between their structure and activity, a number of derivatives differing in the 4-arylazo function were synthesized and evaluated. As shown in Figure 1, the 4-halogenophenyl derivatives **3b**−**6b** have similar inhibitory activities to **1b** (i.e., the analogue with an unsubstituted phenyl ring), while the nonpolar 4-methylphenyl derivative **2b** shows a small decrease in activity. Other

Scheme 1. Synthesis of 4-Arylazo-3,5-diamino-1*H*-pyrazoles

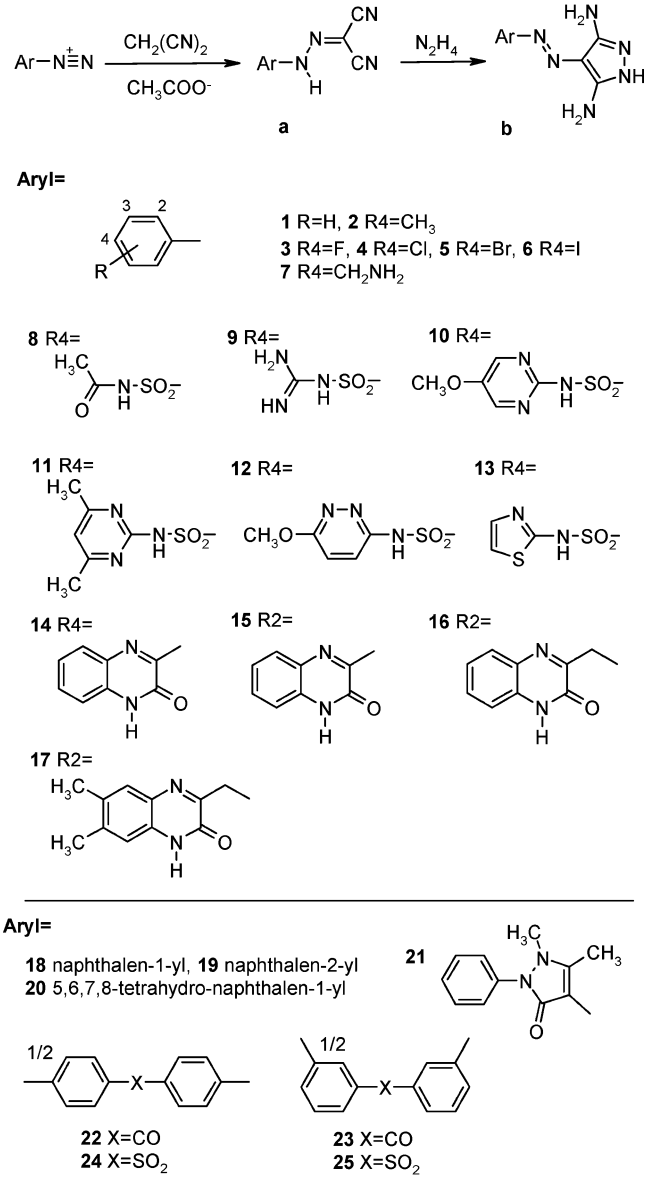

nonpolar substituents also retained the inhibitory activity at the level of **1b**, for example, the comparatively bulky naphthalen-1-yl derivative **18b** (but not the isomeric **19b**) or the partially saturated congener **20b**. Although these data suggest that large aromatic substituents may be compatible with CDK2 inhibitory activity, when other bulky arylamines were used as starting materials, the resulting diaminopyrazoles **8b**−**17b** did not display significant CDK2 inhibitory activity. The explanation for these findings could be related to the nature of the *para* substituent in the arylazo group: a large substituent causing a detrimental effect, probably through steric hindrance. Such an effect is also indicated by the reduced inhibitory activity of the *p*-aminomethyl analogue **7b**. The next subgroup of compounds, **21b**−**24b** obtained from aryldiamines, contained dimeric 3,5-diamino-1*H*-pyrazole systems, so the resulting molecules were much bulkier, and as expected, these derivatives exhibited reduced and insignificant CDK inhibitory activity.

Following the finding that the majority of compounds with at least some activity against CDK2 possessed a small 4-arylazo group, we turned our attention to the effects of various small substituents on the phenyl ring. Specifically, we prepared and tested a series of 4-phenylazo derivatives with an additional

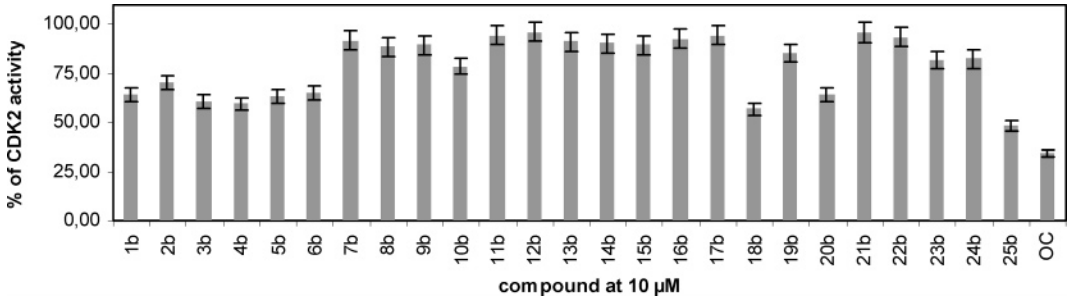

Figure 1. Inhibition of CDK2-cyclin E by 4-arylazo-3,5-diamino-1*H*-pyrazoles at 10 μM concentration; olomoucine (OC) was included as a control. Average values from three determinations ±SD.

Table 1. Inhibition of CDK2 and in Vitro Antiproliferative Activity of Selected Derivatives

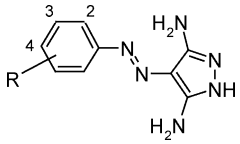

		IC_{50}[a] (μM; or % of viable cells)				
No	R	CDK2	MCF7	HOS	G361	K562
1b	H	22 ± 5	>100 (74 ± 5%)	>100 (83 ± 8%)	>100 (75 ± 2%)	>100 (90 ± 14%)
18b	2-CH=CH−CH=CH-3	10 ± 3	>100 (56 ± 1%)	>100 (79 ± 8%)	>100 (55 ± 14%)	50 ± 3 (7.7 ± 6%)
20b	2-$CH_2CH_2CH_2CH_2$-3	15 ± 6	81 ± 9 (39 ± 10%)	92 ± 5 (32 ± 6%)	77 ± 4 (27 ± 5%)	55 ± 1 (26 ± 7%)
26b	2-NO_2	6.1 ± 1.7	>100 (62 ± 9%)	>100 (57 ± 6%)	>100 (58 ± 2%)	100 ± 10 (48 ± 4%)
27b	3-NO_2	23 ± 2	65 ± 7 (44 ± 6%)	>100 (95 ± 5%)	>100 (69 ± 8%)	79 ± 6 (28 ± 5%)
28b	4-NO_2	40 ± 9	>100 (60 ± 4%)	>100 (80 ± 8%)	>100 (61 ± 10%)	71 ± 6 (25 ± 3%)
29b	2-OH	2.5 ± 0.1	>100 (72 ± 6%)	>100 (84 ± 7%)	>100 (74 ± 12%)	>100 (72 ± 8%)
30b	3-OH	6.0 ± 0.2	>100 (71 ± 9%)	>100 (83 ± 8%)	>100 (70 ± 10%)	>100 (53 ± 6%)
31b	4-OH	3.5 ± 0.7	33 ± 5 (20 ± 6%)	49 ± 9 (22 ± 8%)	64 ± 5 (8.3 ± 4%)	62 ± 8 (23 ± 7%)
32b	2-COOH	92 ± 12	>100 (97 ± 7%)	>100 (91 ± 10%)	>100 (96 ± 12%)	>100 (89 ± 6%)
33b	3-COOH	28 ± 9	>100 (102 ± 8%)	>100 (94 ± 11%)	>100 (93 ± 7%)	>100 (84 ± 8%)
34b	4-COOH	>100	>100 (97 ± 9%)	>100 (92 ± 3%)	>100 (86 ± 14%)	>100 (96 ± 9%)
35b	2-CH_2OH	17 ± 5	>100 (51 ± 10%)	>100 (87 ± 8%)	>100 (84 ± 11%)	>100 (86 ± 2%)
olomoucine		5.0 ± 1.0	134 ± 5	144 ± 15	147 ± 14	145 ± 22

[a] IC_{50} measured in the presence of 15 μM ATP, % of viable cells in the presence of 100 μM of the test compound. Average values from three determinations ±SD.

small polar phenyl substituent (derivatives **26b**−**35b** in Table 1). The most effective members of the series were hydroxy and nitro compounds. In the case of the phenol analogues, the *ortho* (**29b**) and *para* (**31b**) isomers showed the lowest CDK2 IC_{50} values, whereas the *meta*-hydroxy derivative **30b** was about half as potent. Further modification, by insertion of a methylene group between the 2-OH and the phenyl groups (**35b**), led to a decline in activity compared with the homologue **29b**. Interestingly, nitrated compounds **26b**−**28b** displayed a different positional effect. Here, the position of the nitro group affected the CDK2 inhibitory activity in the order *ortho* > *meta* > *para*, with a 2- to 4-fold drop of potency between the different isomers. All carboxylic acids (**32b**−**34b**) drastically lost inhibitory activity.

Mechanism of CDK2 Inhibition. To further investigate the mechanism of CDK2-cyclin E inhibition by the 4-phenylazo-3,5-diamino-1*H*-pyrazole compounds, kinase assays were performed with one of the more potent analogues, **31b**, in which the concentrations of both ATP and the inhibitor were varied. Double reciprocal plots of the data (Figure 2) show that compound **31b** exhibited pure competitive inhibition with respect to ATP, with an apparent K_i value of 13.3 μM, similar to that found with most other known pharmacological CDK inhibitors.

Kinase Selectivity. The selectivity of the most active compounds against CDK2 (i.e., **1b**, **26b**, **27b**, **30b**, **31b**, and **35b**) was then tested against six purified CDKs, including CDK1, CDK4, CDK7, and CDK9 (Table 2). These assays

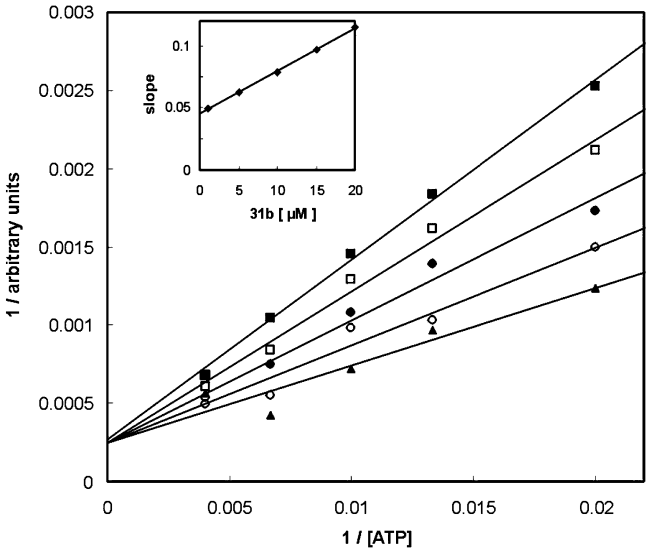

Figure 2. Double reciprocal plot of CDK2-cyclin E activity in the presence of **31b** as a function of ATP concentration. The inhibitor concentrations were 1 μM (filled triangles), 5 μM (empty circles), 10 μM (filled circles), 15 μM (empty squares), and 20 μM (filled squares). The inset shows the secondary replot of slopes vs concentrations of **31b** (K_i = 13.3 μM).

confirmed that phenylazo-3,5-diamino-1*H*-pyrazoles are efficient inhibitors of members of the CDK family other than CDK2. In addition to CDK2-cyclin E, another G1-phase specific kinase,

Table 2. Selectivity of 4-Arylazo-3,5-diaminopyrazoles against Purified Cyclin-Dependent Kinases

	IC_{50}[a]					
compd	CDK1/B	CDK2/E	CDK2/A	CDK4/D1	CDK7/H	CDK9/T1
1b	>100	100	>100	>100	>100	15 ± 3
26b	42 ± 3	22 ± 3	88 ± 1	16 ± 1	77 ± 5	5.6 ± 5
27b	>100	68 ± 6	>100	70 ± 12	>100	12.4 ± 3.2
30b	>100	51 ± 10	>100	56 ±13	82 ± 15	1.5 ± 0.5
31b	44.0 ± 7	20 ± 6	69 ± 1	13.5 ± 3.1	26 ± 13	0.35 ± 0.04
35b	>100	77 ± 5	>100	>100	>100	26 ± 1

[a] Kinase activity assayed in the presence of 100 μM ATP. Average values from three determinations ±SD.

Table 3. Selectivity of **31b** against Various Protein Kinases

protein kinase	kinase activity[a] (%)
CDK9/cyclin T1	6.9
CDK2/cyclin E	31
c-Abl	84
CHK1	89
CK2	65
GSK3β	81
MAPK1	99
p70S6K	51
PKA	67
PKBα	100
SAPK2α	82

[a] In the presence of 10 μM test compound.

CDK4-cyclin D1, was inhibited approximately to the same degree by **26b**, **27b**, **30b**, and **31b**. Structurally related 3-aminopyrazole CDK inhibitors (e.g., PNU-292137), which were identified during the course of our investigation, appear to possess different selectivity profiles and do not inhibit CDK4.[35,36] Interestingly, CDK2 in complex with cyclin A proved to be about 4-fold less-sensitive to the pyrazole derivatives **26b** and **31b** than CDK2-cyclin E. Surprisingly, all of these derivatives were most potent against CDK9-cyclin T1, unlike any other known classes of CDK inhibitors, with **31b** being the most effective inhibitor, with submicromolar potency (IC_{50} = 0.35 μM). The selectivity ratios with respect to CDK9 of the derivative **31b** ranged from 40 to 200 for various other CDKs, suggesting that significant selectivity, even within the CDK family, can be attained with the diaminopyrazole pharmacophore.

To further characterize the pyrazole derivatives, CDK inhibitor **31b** was assayed (at a fixed concentration of 10 μM) against nine other protein kinases, including CDK9 and CDK2 as reference controls (Table 3). Most of the kinases tested were inhibited poorly or not at all, corroborating the selectivity of pyrazole derivatives toward CDKs. Surprisingly, **31b** showed a distinct selectivity profile when compared with other CDK inhibitors. For example, purines also inhibit ERK2 and CDK7,[37−39] whereas paullones and aloisines also inhibit GSK3β.[39,40] Another compound that also reduces CTD phosphorylation of RNAP-II via CDK9 inhibition, 5,6-dichloro-1-β-D-ribofuranosylbenzimidazole (DRB), inhibits casein kinases too,[41,42] an effect not observed with **31b**.

Of the kinases tested, only the structurally distinct ribosomal p70S6 kinase was found to be slightly sensitive to **31b**, with an IC_{50} value of about 10 μM. Although this kinase is one of the potential intracellular targets of the CDK inhibitor purvalanol B, as shown by affinity chromatography,[37] the selectivity profile of **31b** is not reminiscent of any other pharmacological CDK inhibitor, although its cellular kinase specificity profile remains to be determined.

Crystal Structure of 31b with CDK2. The crystal structure of the monomeric CDK2−**31b** complex was determined at 1.80 Å resolution (Supplementary Table 4, Supporting Information) to determine the inhibitor's binding mode within the active site of the kinase and to verify the competitive character of the inhibition. As expected, **31b** binds to the ATP site located in the cleft between the N- and C-terminal kinase domains (Figure 3a). The inhibitor is oriented with the 3,5-diaminopyrazole system facing the CDK2 hinge region polypeptide backbone, where it interacts with Glu81 and Leu83 through three H-bonds (Figure 3b), in a manner similar to that of other heterocyclic CDK inhibitors.[43] The phenylazo moiety faces the Phe80 phenyl ring, forming a π interaction and the phenol function H-bonding to the carboxyl of Asp145 (Figure 3b). The orientation and the H-bond pattern of **31b** in the active site corresponds to those of PNU-292137, recently described as a selective CDK2 inhibitor.[35,36] Interestingly, **31b** is observed to adopt a conformation close to a coplanar *cis*-diaryldiazine (Figure 3c). The energetically less-favorable *cis* ligand conformation, compared to the *trans* arrangement, appears to be preferred because it enables simultaneous interaction with the diaminopyrazole and phenol moieties described above. Diaryldiazines can undergo facile *cis*−*trans* isomerization under a variety of conditions and by several mechanisms; whereas *trans*-diaryldiazines exist predominantly in planar conformations, this is not possible in the *cis* geometry, where the two aryl systems are not coplanar.[44] The electron density for **31b** in the CDK2 complex is well-defined apart from the phenol substituent, where weak density is observed for the benzene ring and density for the OH group is absent. We suggest that this situation is due to the fact that the electron density represents an average picture of two binding modes, in which the ligand adopts *cis* conformations with the phenol group either above or below the plane of the remaining aryldiazine system.

Model of 31b Complexed to CDK9. The selectivity of **31b** toward CDK9-cyclin T1 found during kinase assays prompted an investigation into the structural basis for this selectivity. Analysis of the modeled interactions between **31b** and CDK9 (Figure 3b) indicates the participation of Asp167 (which corresponds to Asp145 in CDK2) in an H-bond with the phenol-OH of **31b**. H-bond interactions corresponding to those with Glu81 and Leu83 observed in the CDK2-**31b** complex appear to be absent in the CDK9-**31b** model. This is the first CDK inhibitor to show no participation of the molecular fork of CDK in intermolecular hydrogen bonds, previously described to be present in intermolecular hydrogen bonds in the structures of all CDK−inhibitor complexes studied so far.[45] In the CDK9 complex structure, CDK9 interactions with **31b** are characterized by predominantly hydrophobic and van der Waals interactions between the protein and the 4-phenylazo moiety. Most of the intermolecular contacts between CDK9 and **31b** involve a hydrophobic pocket formed by the residues Ile25, Val33, Phe103, Cys116, Leu156, Ala166, and Asp167. A direct structural comparison of both binary complexes indicates that the high specificity of **31b** for CDK9 does not stem from the establishment of H-bonds, because the CDK9−**31b** complex presents a smaller number of H-bonds than the CDK2−**31b** complex. The most striking difference between the two complexes concerns the intermolecular contact area, which is significantly higher in the CDK9 complex (190 Å^2) than in the CDK2 complex (174 Å^2; Figure 3d,e). Structural inspection of the interaction between **31b** and CDK9 suggests that the inhibitor's specificity against CDK9 is probably due to the 4-phenylazo moiety, which affords a higher intermolecular

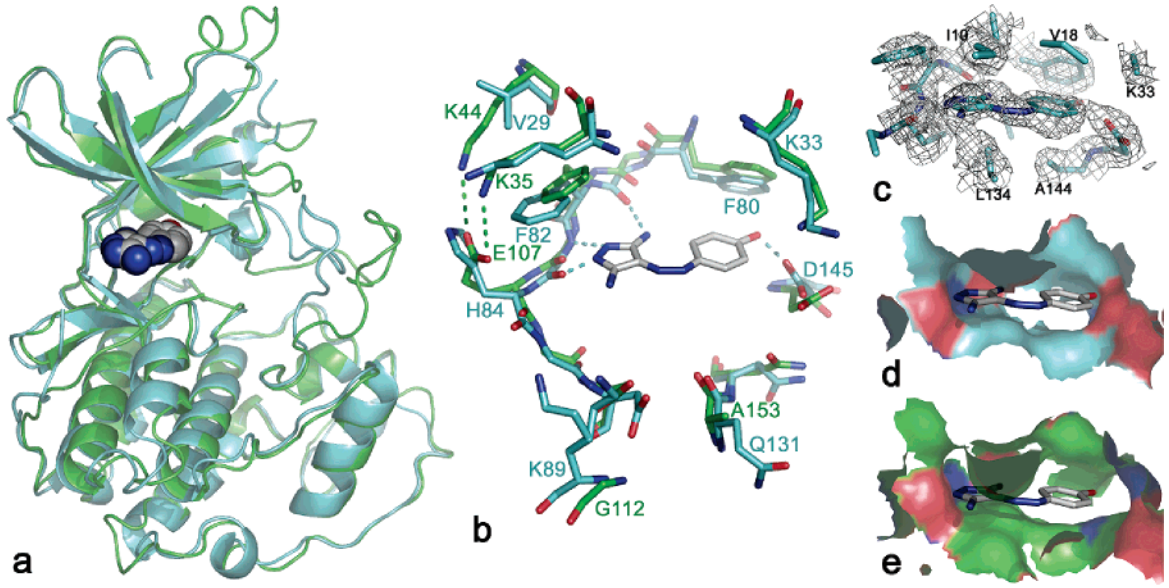

Figure 3. Crystal structure of CDK2 complex with **31b**. (**a**) The experimentally determined 3D structure of CDK2 (cyan) aligned with the modeled structure of CDK9 (green); the ligand is shown as a space-filling CPK representation. (**b**) Details of the interactions between ligand and residues of the ATP-binding pocket, indicated with broken lines. (**c**) Observed electron density around the bound inhibitor **31b**. The protein surfaces within 4 Å of the ligand are shown for CDK2 (**d**) and CDK9 (**e**), respectively.

contact area with CDK9 than that observed for the CDK2−**31b** complex. Especially interesting is the presence of two salt bridges (Glu107−Lys35 and Glu107−Lys44) in the CDK9−**31b** structure; these were also observed in the CDK9−flavopiridol complex and involve residues from two different lobes of the CDK9 structure.[45] This strong electrostatic interaction brings the two lobes of CDK9 closer together, which increases the contact area between the enzyme and the inhibitor. These salt bridges are not observed in the CDK2−**31b** complex. A tighter ATP-binding pocket observed in the CDK9−**31b** complex makes possible a higher number of intermolecular van der Waals contacts between CDK9 and **31b**.

Cellular Activity. The 4-phenylazo-3,5-diamino-1*H*-pyrazoles with the most potent CDK inhibitory activity were tested for antiproliferative activity against four human tumor cell lines of different histological origins. The results are summarized in Table 1. All compounds except derivatives **27b**, **28b**, **31b**, and **20b** showed only marginal effects, with IC_{50} values exceeding 100 μM. This weak activity is comparable with that of olomoucine, a well-known but weak inhibitor of CDK1 and CDK2.[46] In general, derivatives substituted with bulky aryl moieties (e.g., sulfonamides **8b**−**13b** or bis-azo derivatives **22b**−**25b**, data not shown) showed either very low or no antiproliferative activity, while some pyrazoles with smaller 4-aryl side chains displayed measurable IC_{50} values.

Surprisingly, the observed effects of the position of the hydroxyl- and nitro-phenyl substituents on the activity did not simply reflect the CDK inhibition pattern. Hydroxy compounds **29b** and **31b**, among the most potent CDK2 inhibitors, showed significant differences in cell proliferation assays. Compound **31b** caused significant reductions in cell number in all four cell lines used. In contrast, **29b** and **30b**, despite their potent CDK inhibition, caused much weaker responses. Conversely, the nitro derivatives **26b** and **28b**, which differed approximately 7-fold in CDK inhibition potency, induced cell death at comparable concentrations.

Notably, compound **20b**, which has a weak impact on CDK activity, also showed antiproliferative activity, exceeding that of the olomoucine control on all tested cell lines, probably due to its relatively low polar surface area, which may facilitate membrane penetration and alter its enzyme binding parameters. In summary, the observed discrepancies between the results of the kinase and cellular assays suggest that the pyrazole compounds' effects on targets other than CDKs may contribute to their antiproliferative activity and/or that their physicochemical properties affect their cellular activities.

Cell Cycle Effects. It is well known that CDK2 and CDK4 play critical roles in the G1-S transition of the cell cycle by phosphorylating the retinoblastoma protein (pRb), which in turn activates E2F-mediated transcription of S-phase specific genes.[47] Inhibition of cellular CDK activity is, therefore, expected to result in inhibition of pRb phosphorylation and cell cycle arrest in the G1 phase. To investigate further the cellular effects of the 4-arylazo-3,5-diamino-1*H*-pyrazoles, we therefore evaluated compound **31b** (an analogue with strong anti-CDK and growth inhibition activities and high selectivity) using cell cycle analysis and expression−phosphorylation assays in cancer cells. The antiproliferative activity of **31b** was verified by flow cytometric analysis of subconfluent and asynchronously growing HT-29 cells, which were doubly stained with propidium iodide and 5-bromo-2′-deoxyuridine (BrdU). In accordance with the selectivity of **31b** toward CDK9-cyclin T1 when measured in vitro, this compound did not influence the cell cycle, unlike the less-selective CDK inhibitor roscovitine, which blocked both G1-S and G2-M transitions (Figure 4). With **31b**, we only observed a difference in the S-phase cell population, which showed substantially reduced intensity of the BrdU signal compared with control cells. Subsequently, increases in the sub-G1 cell population, usually considered apoptotic, were observed in cells treated with either **31b** or roscovitine for periods longer than 3 h.

When MCF7 cells were treated with varying concentrations of **31b** for 24 h, dose-dependent inhibition of pRb phosphorylation at Ser807 and Ser780 (both of which are specifically phosphorylated during the G1 phase of the cell cycle by CDK4-cyclin D) and Thr821 (specifically phosphorylated by CDK2-cyclin E) was observed in immunoblots of total proteins probed with phosphospecific antibodies (Figure 5). The results demonstrate the ability of **31b** to affect the activities of CDK4 and CDK2 in cells. In addition, a drop in pRb phosphorylation

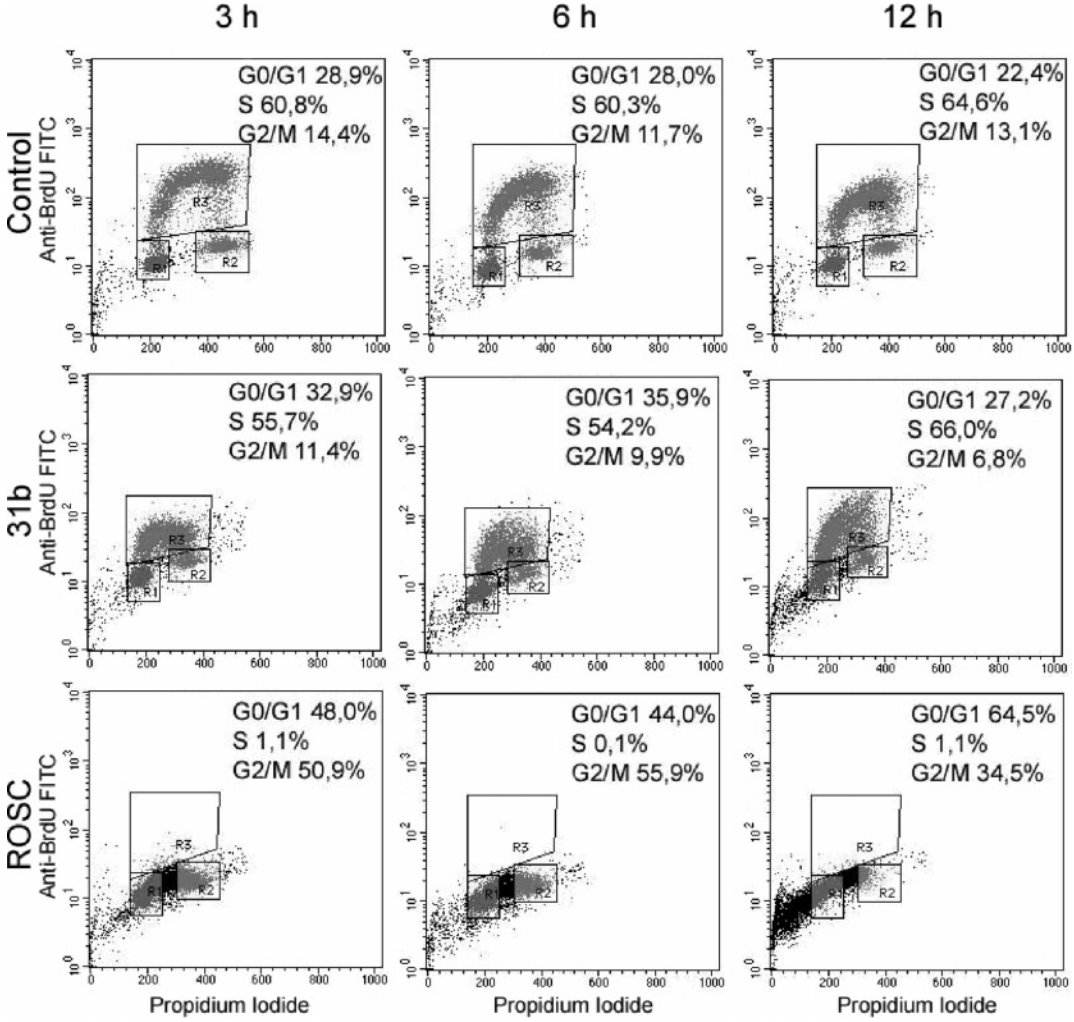

Figure 4. Cell cycle analysis and BrdU incorporation in HT-29 cells treated with **31b** (50 μM) or roscovitine (70 μM). Drug concentrations were equivalent to IC_{50} values of the compounds against HT-29 cells.

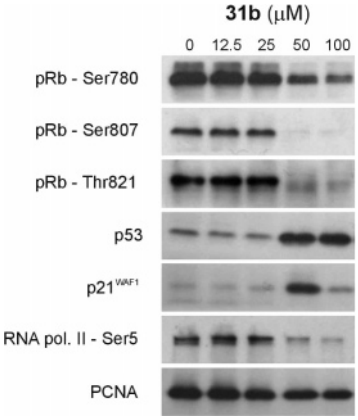

Figure 5. Immunoblot analysis of MCF7 cells treated for 24 h with the indicated concentrations of **31b**. Phosphorylation of pRb appears to be reduced at Ser780 and Ser807 (indicative of decreased activity of CDK4) and Thr821 (indicative of decreased activity of CDK2) by **31b**. In addition, the compound appears to induce increases in the levels of the tumor suppressor protein p53 and $p21^{WAF1}$ and to reduce the phosphorylation of CTD of RNA polymerase II, indicating that it induces blocks in transcription.

occurred at inhibitor concentrations between 25 and 50 μM, in accordance with the observed IC_{50} value for MCF7 growth inhibition (Table 1). However, due to the marked selectivity of **31b** toward CDK7 and CDK9, we surmise that decreased phosphorylation of pRb may be caused by insufficient activity of CDK4 and CDK2 (blocked activation by CDK7, absence of cyclins) rather than by direct inhibition.

Inhibition of Transcription. Pharmacological CDK inhibitors usually increase the cellular level of the tumor suppressor protein p53 and, consequently, transcription of p53-activated genes.[24,48] This effect probably results from direct inhibition of CDKs involved in the regulation of transcription, that is, CDK7, CDK8, and CDK9, which leads to decreased levels of short-lived mRNA and protein gene product. One such mRNA encodes the negative regulator p53-specific Hdm2 ubiquitin E3 ligase. Insufficient elongation of the ligase triggers stabilization of the p53 protein, as demonstrated by cell treatment with certain CDK inhibitors.[24,32,48] Paradoxically, a block in transcription can thus be accompanied by increased levels of certain proteins, like p53 and its downstream regulated tumor suppressor $p21^{WAF1}$. We, therefore, evaluated the effect of the derivative **31b** at various concentrations on the levels of p53 and $p21^{WAF1}$ proteins in MCF7 cells and found that 24 h incubation with **31b** at concentrations of 50 and 100 μM resulted in strongly increased levels of p53 (Figure 5). Accumulated p53 then transactivated the cell cycle inhibitory protein $p21^{WAF1}$, levels of which were maximal at 50 μM **31b**. In addition, the activity of **31b** was significant at concentrations close to the IC_{50} value for MCF7 growth inhibition. Thus, increased levels of $p21^{WAF1}$ may also contribute to inhibition of CDKs in cells. Olomoucine, tested in parallel as a control, was effective at doses of about 100 μM (data not shown).

Table 4. Inhibition of mRNA Synthesis by Compound **31b** (50 μM) or Roscovitine (70 μM) in HT-29 Cells[a]

GAPDH copies/10^6 cells[b]

	0 h	3 h	6 h	12 h
control	2 124 368	4 096 055	1 395 413	3 030 440
	±399 147	±906 931	±233 769	±230 709
roscovitine	ND	3 945 095	3 146 605	3 926 015
	ND	±446 126	±898 073	±965 476
31b	ND	3 342 533	3 785 908	1 811 960
	ND	±334 107	±479 616	±581 162

CEA copies/10^6 cells[b]

	0 h	3 h	6 h	12 h
control	26 030	34 053	14 235	18 630
	±3236	±2409	±1568	±2506
roscovitine	ND	30 568	19 150	24 350
	ND	±3005	±4801	±8988
31b	ND	27 900	22 620	12 005
	ND	±3690	±816	±4123

EpCAM copies/10^6 cells[b]

	0 h	3 h	6 h	12 h
control	4 238 025	8 732 195	2 609 440	4 888 343
	±162 292	±398 172	±362 215	±531 734
roscovitine	ND	8 258 813	6 151 085	6 863 365
	ND	±788 357	±404 186	±16 636
31b	ND	6 047 138	5 069 600	2 951 620
	ND	±485 595	±471 663	±121 527

[a] After the indicated period, total RNA was extracted and absolute numbers of GAPDH, CEA, and EpCAM gene transcripts were quantified by real-time PCR. Drug concentrations were equivalent to IC_{50} values for the inhibitors against HT-29 cells. [b] Average values from four determinations ±SD.

The CDK inhibitor roscovitine has also been reported to inhibit mRNA synthesis, possibly through inhibition of CDK7 and CDK9, which phosphorylate the CTD of RNAP-II and thus activate transcription.[22,25] The possibility that **31b** could lead to a loss of phosphorylation of RNAP-II in cells was assessed by Western blot analysis with phosphospecific CTD antibodies. Figure 5 shows there was a concentration-dependent decrease of Ser5 phosphorylation of RNAP-II in MCF7 cells treated with **31b** for 24 h. Moreover, two epithelial genes, encoding carcinoembryonic antigen (CEA) and human epithelial cell adhesion molecule (EpCAM), and one housekeeping gene, encoding glyceraldehyde-3-phosphate dehydrogenase (GAPDH), were selected for analysis of transcriptional inhibition using quantitative real-time PCR (RQ RT-PCR) in the HT-29 colon cancer cell line (Table 4). Copy numbers of GAPDH, CEA, and EpCAM mRNAs decreased in a time-dependent manner when incubated with either **31b** at 50 μM or roscovitine at 70 μM. However, **31b** was much more potent in this respect, which is consistent with its direct inhibition of CDK9-cyclin T1.

Conclusions

The most potent pyrazole derivative from the series presented here was 4-[(3,5-diamino-1*H*-pyrazol-4-yl)diazenyl]phenol **31b** (designated CAN508), which selectively inhibited CDK9 kinase in vitro. The derivative proved to be a competitive inhibitor of CDK2-cyclin E with respect to ATP. Cellular activity of **31b** blocks proliferation of several tested cancer cell lines. Despite **31b** having high specificity toward CDK9-cyclin T1, its inhibition does not seem to be the sole reason for the induction of p53 and the observed antiproliferative potency. The well-known CDK inhibitor roscovitine, which has similar affinity for CDK9,[11,32,38] causes accumulation of p53 in cells treated at concentrations lower than **31b**.[32,48] A comparison of the CDK selectivity profiles suggests that inhibition of other kinases (probably via combined effects on CDK2, CDK7, and CDK9) may be responsible for the antiproliferative and pro-apoptotic potency of CDK inhibitors. However, the cellular activity of several 4-phenylazo-3,5-diamino-1*H*-pyrazole derivatives significantly exceeded that of olomoucine, thus, they represent good starting points for further structural optimization of specific CDK9 inhibitors, with potential pharmacological applications in oncology and virology.

Experimental Section

General. All compounds prepared were homogeneous, according to thin-layer chromatographic analysis. Elemental analyses were performed with an EA elemental analyzer (Fisons Instruments). Melting points were determined using a Boetius stage apparatus and are not corrected. All reaction solvents and reagents were purchased from Sigma-Aldrich, unless specified otherwise. Specific antibodies were purchased from Cell Signaling (total pRb and pRb phosphorylated at Ser780 and Ser807), Biosource (pRb phosphorylated at Thr821), Abcam (RNA polymerase II phosphorylated at Ser5), and Becton−Dickinson (anti-BrdU-FITC conjugate) or were generous gifts from B. Vojtěšek (p53, PCNA, $p21^{WAF1}$).

General Method for Preparing Hydrazones a. The appropriate amine (5 mmol) was dissolved in a mixture of water (30 mL) and hydrochloric acid (4.5 mL of 37% w/v soln). A solution of $NaNO_2$ (0.35 g, 5 mmol) in ice-cold water (5 mL) was added dropwise with stirring to the cooled amine solution (0−5 °C). The diazonium salt solution so formed was then added dropwise to a solution of malononitrile (0.5 g, 7.5 mmol) and NaOAc (12.5 g) in water (50 mL) with continuous stirring and cooling. After adding the diazonium salt, the reaction mixture was stirred and cooled for an additional 30 min before being placed in a refrigerator overnight. The following day, the precipitated hydrazone product was filtered, washed with water, and dried. Yields were between 90 and 100% (for details see the Supporting Information). For the preparation of compounds **32a**−**35a**, twice the above quantities of hydrochloric acid, $NaNO_2$, malononitrile, and NaOAc were used.

General Method for Preparing Pyrazoles b. A solution of hydrazine hydrate (0.5 g, 9 mmol) in MeOH (30 mL) was added to the hydrazone **a** (3 mmol). The reaction mixture was heated under reflux for 4 h and was then evaporated to dryness. The solid residue was recrystallized from appropriate solvents (for details see Supplementary Table 2, Supporting Information). Compounds **13b** and **14b** were precipitated from aqueous solution by acidification with hydrochloric acid to pH = 1.

Enzyme Inhibition Assay. CDK2-cyclin E kinase was produced in Sf9 insect cells co-infected with appropriate baculoviral constructs, as previously described.[29] The enzyme was purified on a NiNTA column (Qiagen) and assayed with 1 mg/mL histone H1 in the presence of 15 μM ATP, 0.05 μCi [γ-^{33}P]ATP and of the test compound in a final volume of 10 μL, all in reaction buffer (50 mM HEPES, 10 mM $MgCl_2$, 5 mM EGTA, 10 mM 2-glycerolphosphate, 1 mM NaF, 1 mM DTT, pH 7.4). After a 10 min incubation, reactions were stopped by adding 5 μL of 3% aq H_3PO_4. Aliquots were spotted onto P-81 phosphocellulose (Whatman), which was subsequently washed 3× with 5% aq H_3PO_4 and finally air-dried. To quantify kinase inhibition, a BAS-1800 digital image analyzer (Fujifilm) was employed. Kinase activity was expressed as a percentage of maximum activity. The concentration of the test compounds required to decrease the CDK activity by 50% was determined from dose−response curves and designated IC_{50}. For the kinetic analyses, the activity was expressed as arbitrary units (AU) of digital image analyzer signal.

Kinase Selectivity. CDK selectivity was evaluated using a panel of purified kinases (CDK1-cyclin B, CDK2-cyclin A, CDK4-cyclin D1, CDK7-cyclin H, and CDK9-cyclin T1), as previously described.[38,49] Other protein kinase activities were measured in duplicates at a single fixed concentration of **31b** (10 μM): c-Abl, CHK1, GSK3β, p70S6K, PKA and PKBR were assayed in 8 mM MOPS, pH 7.0, 0.2 mM EDTA, MAPK1 and SAPK2α in 25 mM Tris, pH 7.5, 0.02 mM EGTA, and CK2 in 20 mM HEPES, pH

7.6, 0.15 M NaCl, 0.l mM EDTA, 2 mM DTT, 0.1% Triton X-100, all with 10 mM Mg-acetate, 10 μM ATP, [γ-^{33}P]ATP (500 cpm/pmol) and appropriate peptide substrates for 40 min. The reactions were stopped by adding 5 μL of 3% aq H_3PO_4. Aliquots were then spotted onto a P30 filtermat and washed 3× with 5% aq H_3PO_4 and air-dried prior to scintillation counting.

Crystallization and Structure Determination. Human recombinant CDK2 was expressed, purified, and crystallized as previously described.[43,50] Data were collected at the Cyclacel home source using a R-AXIS IV++ image plate (Rigaku). Data processing was carried out using programs from the d*TREK software suite.[51] The structures were solved by molecular replacement using MOLREP[52] and PDB entry 1PW2 as the search models for CDK2. ARP/wARP[53] was used for the addition of water molecules, and REFMAC[52] was used for structural refinement. A number of rounds of refinement and model building with the program Quanta (Accelrys) were carried out. Crystallographic data and statistics are summarized in Supplemetary Table 4 (Supporting Information). The structure has been deposited with the Protein Data Bank (PDB) under the accession code 2CLX.

Molecular Model of the CDK9−31b Complex. A previously published protocol was used to model the binary CDK9−**31b** complex.[45] Briefly, the atomic coordinates for CDK2−**31b** were used as the starting points for modeling the CDK9−**31b** complex. Therefore, the final model of the complex includes the atomic coordinates of the inhbitor **31b**. This has been confirmed by computational docking studies using PRINCIANE (http://www.biocristalografia.df.ibilce.unesp.br/princiane/). Fifteen residues from the N-terminus and 45 from the C-terminus were removed from the CDK9 model because there is no good template for these fragments. The webserver Parmodel was used to generate all models for the CDK9−**31b** complex.[54] Several slightly different models can be calculated by varying the initial structure. We generated 1000 models for the CDK9−**31b** complex, and the final models were selected based on stereochemical quality. The optimization of the complex was carried out by the use of the variable target function method, followed by 500 steps of conjugate gradient minimization using Parmodel.[54] All optimization processes were performed on a Beowulf Cluster (BioComp, S. J. do Rio Preto, Brazil). The overall stereochemical quality of the final model for the complex of CDK9−**31b** was assessed by the program Parmodel.[54] Analysis of the stereochemical quality of the final model of the CDK9 indicates that 98.6% nonglycine residues lie in the most favored and additional allowed regions of the Ramachandran plot and only 1.4% lie in the generously allowed regions. Root-mean-square (rms) differences from ideal geometries for bond lengths and angles were calculated with Parmodel.[54] Overall deviations from ideal geometry are 0.025 Å for bond distances and 2.51° for bond angles.

Cell Maintenance and Growth Inhibition Assay. The ability of the test substances to inhibit cancer cell growth was determined in vitro with K562, MCF7, HOS, and G361 cell lines. The cells, cultured in DMEM (supplemented with 10% fetal calf serum, 4 mM glutamine, 100 IU/mL penicillin, 100 μg/mL streptomycin) in a humidified CO_2 incubator at 37 °C, were redistributed into 96-well microtiter plates at appropriate densities for their respective cell sizes and growth rates. After a 12 h preincubation, test compounds in 6-fold dilutions were added. Treatment (in the 1−100 μM range) lasted for 72 h. At the end of this period, the cells were fed for 1 h with Calcein AM, and the fluorescence of the live cells was measured at 485 nm/538 nm (ex/em) with a Fluoroskan Ascent reader (Labsystems). IC_{50} values, the drug concentrations lethal to 50% of the cancer cells, were determined from the dose−response curves.

Immunoblotting. For direct immunoblotting, total cellular protein lysates were prepared by harvesting treated cells in Laemmli sample buffer. Proteins were separated on 10% SDS-polyacrylamide gels and electroblotted onto nitrocellulose membrane. The blotted membranes were stained with Ponceau-S in 1% aq AcOH to verify equal protein loading, destained, and blocked in PBS and 0.1% Tween 20 (PBS-T) with 5% low fat milk. The membranes were then incubated with specific antibodies overnight. After washing three times in PBS-T, the membranes were incubated with a 1:2000 dilution of peroxidase-conjugated secondary antibodies. After another three washes in PBS-T, peroxidase activity was detected using ECL+ reagents (AP Biotech) according to the manufacturer's instructions.

BrdU Incorporation and Cell Cycle Analysis. Subconfluent HT29 cells were treated with **31b** or roscovitine at concentrations corresponding to IC_{50} values (50/70 μM) for 3, 6, and 12 h. The cultures were fed a pulse of 10 μM 5-bromo-2′-deoxyuridine (BrdU) for 30 min at 37 °C before harvesting. The cells were trypsinized, fixed with ice-cold 70% ethanol, incubated on ice for 30 min, washed with PBS, and resuspended in 2 M aq HCl for 30 min at room temperature to denature their DNA. Following neutralization with 0.1 M $Na_2B_4O_7$, the cells were harvested by centrifugation and washed with PBS containing 0.5% Tween-20 and 1% BSA. They were then stained with anti-BrdU FITC-labeled antibody (1:50, Becton-Dickinson) for 30 min at room temperature in the dark. The cells were then washed with PBS, incubated with propidium iodide (0.1 mg/mL) and RNAse A (0.5 mg/mL) for 1 h at room temperature in the dark, and finally analyzed by flow cytometry using a 488 nm single beam laser (FACSCalibur, Becton Dickinson).

RNA Isolation and Reverse Transcription. Total RNA was extracted from treated/control HT-29 cells (5×10^6) cultured in 6-well panels with TRI reagent (Molecular Research Center, Cincinnati, OH) according to the manufacturer's instructions. The concentration and purity of isolated RNA was assessed by UV spectroscopy. Three microgram portions of total RNA were used for reverse transcription in a final volume of 30 μL. The RNA solution was preincubated with 0.3 μg of random primers (Promega) at 70 °C for 5 min and immediately placed on ice. Then, 6 μL of 5× RevertAid reverse transcriptase buffer (Fermentas), 3 μL of 10 mM deoxyribonucleotide triphosphates (dNTPs), and 0.75 μL of 40 U/μL RNAsin ribonuclease inhibitor (Promega) were added, and the mixtures were incubated for 5 min at room temperature. In the final step, 150 U of RevertAid Moloney murine leukaemia virus reverse transcriptase (Fermentas) was added to each tube, the samples were incubated at 42 °C for 60 min, and the reverse transcriptase was then heat-inactivated at 95 °C for 5 min.

Real-Time Polymerase Chain Reaction (RQ RT-PCR). Two epithelial genes, encoding CEA (CEACAM5) and human EpCAM (TACSTD 1), and one housekeeping gene, encoding GAPDH, were selected for analysis of transcriptional inhibition using quantitative real-time PCR. Primers were selected using PrimerPremier3 software and NCBI reference sequences (accession numbers NM_004363, NM_002354, and NM_002046, respectively). Specific primers from two different exons and probes (Generi-Biotech, Czech Republic) to span introns were designed to reduce amplification of genomic DNA. The following primers and probes were used: CEA3 5′-TAA GTG TTG ACC ACA GCG ACC C-3′, CEA4 5′-GTT CCC ATC AAT CAG CCA AGA A-3′, CEA probe 5′-ATG TCC TCT ATG GCC CAG ACG ACC C-3′-BHQ1-HEX; EpCAM3 5′-AAA CAC AAA GCA AGA GAA AAA CCT-3′, EpCAM4 5′-AAT TTT GGA TCC AGT TGA TAA CG-3′, EpCAM probe 5′-TTG CGG ACT GCA CTT CAG AAG GA-3′-BHQ1-HEX; GAPDH−F 5′-GAA GAT GGT GAT GGG ATT TC-3′, GAPDH-R 5′-GAA GGT GAA GGT CGG AGT-3′, GAPDH probe 5′-CAA GCT TCC CGT TCT CAG CC-3′-BHQ1-FAM. RQ RT-PCR reactions were performed in 25 μL reaction volumes consisting of 1 U of HotStart Taq polymerase, 3 mM $MgCl_2$, 10× PCR buffer (AB Gene), 200 μM dNTPs (Promega), 100 ng DNA, and variable amounts of primer/probe: 300 nM CEA3, 600 nM CEA4, and 200 nM CEA probe; 400 nM EpCAM3, 400 nM EpCAM4, and 200 nM EpCAM probe; 300 nM GAPDH-F, 300 nM GAPDH-R, and 200 nM GAPDH probe. The optimized thermal profiles for amplification involved 15 min Taq polymerase activation at 96 °C, followed by 50 cycles at 95 °C for 15 s and 65 °C for 15 s (CEA), 50 cycles at 95 °C for 15 s and 59 °C for 15 s (EpCAM), and 50 cycles at 95 °C for 15 s and 60 °C for 30 s (GAPDH). Gene expression was quantified from calibration curves

using appropriately diluted gene specific amplicons ranging between 30 and 1 000 000 copies per reaction. Each sample was analyzed in duplicate. Positive and negative controls were also incorporated into each experiment to evaluate reproducibility and possible sample contamination during the PCR procedure.

Acknowledgment. The authors thank K. Faksová, E. Hirnerová, J. Hudcová, and the screening group members at Cyclacel for their contributions. B. Vojtěšek is acknowledged for the gift of antibodies and Sees-editing for English corrections. The work was supported by GACR Grant 204/03/D231, MSMT Grant 6198959216, and SMOLBnet FAPESP 01/07532-0. W.F.A. is a researcher for the Brazilian Council for Scientific and Technological Development, CNPq.

Supporting Information Available: Data from the elemental analyses, melting points, recrystallization solvents of newly prepared compounds, references to previously known compounds, as well as X-ray data are included. This material is available free of charge via the Internet at http://pubs.acs.org.

References

(1) Morgan, D. O. Cyclin-dependent kinases: engines, clocks, and microprocessors. *Annu. Rev. Cell Dev. Biol.* **1997**, *13*, 261−291.
(2) Sherr, C. J. Cancer cell cycles. *Science* **1996**, *274*, 1672−1677.
(3) Sielecki, T. M.; Boylan, J. F.; Benfield, P. A.; Trainor, G. L. Cyclin-dependent kinase inhibitors: useful targets in cell cycle regulation. *J. Med. Chem.* **2000**, *43*, 1−18.
(4) Dai, Y.; Grant, S. Cyclin-dependent kinase inhibitors. *Curr. Opin. Pharmacol.* **2003**, *3*, 362−370.
(5) Fischer, P. M.; Lane, D. P. Inhibitors of cyclin-dependent kinases as anti-cancer therapeutics. *Curr. Med.* Chem. **2000**, *7*, 1213−1245.
(6) Knockaert, M.; Greengard, P.; Meijer, L. Pharmacological inhibitors of cyclin-dependent kinases. *Trends Pharmacol. Sci.* **2002**, *23*, 417−425.
(7) Hirai, H.; Kawanishi, N.; Iwasawa, Y. Recent advances in the development of selective small molecule inhibitors for cyclin-dependent kinases. *Curr. Top. Med. Chem.* **2005**, *5*, 167−179.
(8) McInnes, C.; Fischer, P. M. Strategies for the design of potent and selective kinase inhibitors. *Curr. Pharm. Des.* **2005**, *11*, 1845−1863.
(9) Fischer, P. M. The design of drug candidate molecules as selective inhibitors of therapeutically relevant kinases. *Curr. Med. Chem.* **2004**, *11*, 1563−1583.
(10) Fischer, P. M.; Gianella-Borradori, A. Recent progress in the discovery and development of CDK inhibitors. *Expert Opin. Invest. Drugs* **2005**, *14*, 457−477.
(11) Benson, C.; Kaye, S.; Workman, P.; Garrett, M.; Walton, M.; de Bono, J. Clinical anticancer drug development: targeting the cyclin-dependent kinases. *Br. J. Cancer* **2005**, *92*, 7−12.
(12) Loyer, P.; Trembley, J. H.; Katona, R.; Kidd, V. J.; Lahti, J. M. Role of CDK/cyclin complexes in transcription and RNA splicing. *Cell. Signalling* **2005**, *17*, 1033−1051.
(13) Schang, L. M. Advances on cyclin-dependent kinases (CDKs) as novel targets for antiviral drugs. *Curr. Drug Targets: Infect. Disord.* **2005**, *5*, 29−37.
(14) Fischer, P. M. Cyclin-dependent kinase inhibitors: discovery, development and target rationale for different therapeutic applications. *Drugs Future* **2005**, *30*, 911−929.
(15) Chao, S.-H.; Fujinaga, K.; Marion, J. E.; Taube, R.; Sausville, E. A.; Senderowicz, A. M.; Peterlin, B. M.; Price, D. H. Flavopiridol inhibits P-TEFb and blocks HIV-1 replication. *J. Biol. Chem.* **2000**, *275*, 28345−28348.
(16) Schang, L. M. Effects of pharmacological cyclin-dependent kinase inhibitors on viral transcription and replication. *Biochim. Biophys. Acta* **2004**, *1697*, 197−209.
(17) Agbottah, E.; de La Fuente, C.; Nekhai, S.; Barnett, A.; Gianella-Borradori, A.; Pumfery, A.; Kashanchi, F. Antiviral Activity of CYC202 in HIV-1-infected Cells. *J. Biol. Chem.* **2005**, *280*, 3029−3042.
(18) Heredia, A.; Davis, C.; Bamba, D.; Le, N.; Gwarzo, M. Y.; Sadowska, M.; Gallo, R. C.; Redfield, R. R. Indirubin-3′-monoxime, a derivative of a Chinese antileukemia medicine, inhibits P-TEFb function and HIV-1 replication. *AIDS* **2005**, *19*, 2087−2095.
(19) Fischer, P. M. The use of CDK inhibitors in oncology: a pharmaceutical perspective. *Cell Cycle* **2004**, *3*, 742−746.
(20) Ortega, S.; Prieto, I.; Odajima, J.; Martin, A.; Dubus, P.; Sotillo, R.; Barbero, J. L.; Malumbres, M.; Barbacid, M. Cyclin-dependent kinase 2 is essential for meiosis but not for mitotic cell division in mice. *Nat. Genet.* **2003**, *35*, 25−31.
(21) Tetsu, O.; McCormick, F. Proliferation of cancer cells despite CDK2 inhibition. *Cancer Cell* **2003**, *3*, 233−245.
(22) Ljungman, M.; Paulsen, M. T. The cyclin-dependent kinase inhibitor roscovitine inhibits RNA synthesis and triggers nuclear accumulation of p53 that is unmodified at Ser15 and Lys382. *Mol. Pharmacol.* **2001**, *60*, 785−789.
(23) Chao, S.-H.; Price, D. H. Flavopiridol inactivates P-TEFb and blocks most RNA polymerase II transcription in vivo. *J. Biol. Chem.* **2001**, *276*, 31793−31799.
(24) Demidenko, Z. N.; Blagosklonny, M. V. Flavopiridol induces p53 via initial inhibition of Mdm2 and p21 and, independently of p53, sensitizes apoptosis-reluctant cells to tumor necrosis factor. *Cancer Res.* **2004**, *64*, 3653−3660.
(25) Whittaker, S. R.; Walton, M. I.; Garrett, M. D.; Workman, P. The cyclin-dependent kinase inhibitor CYC202 (R-roscovitine) inhibits retinoblastoma protein phosphorylation, causes loss of cyclin D1, and activates the mitogen-activated protein kinase pathway. *Cancer Res.* **2004**, *64*, 262−272.
(26) MacCallum, D. E.; Melville, J.; Frame, S.; Watt, K.; Anderson, S.; Gianella-Borradori, A.; Lane, D. P.; Green, S. R. Seliciclib (CYC202, R-roscovitine) induces cell death in multiple myeloma cells by inhibition of RNA polymerase II-dependent transcription and down-regulation of Mcl-1. *Cancer Res.* **2005**, *65*, 5399−5407.
(27) Lacrima, K.; Valentini, A.; Lambertini, C.; Taborelli, M.; Rinaldi, A.; Zucca, E.; Catapano, C.; Cavalli, F.; Gianella-Borradori, A.; MacCallum, D. E.; Bertoni, F. In vitro activity of cyclin-dependent kinase inhibitor CYC202 (Seliciclib, R-roscovitine) in mantle cell lymphomas. *Ann. Oncol.* **2005**, *16*, 1169−1176.
(28) Shan, B.; Zhuo, Y.; Chin, D.; Morris, C. A.; Morris, G. F.; Lasky, J. A. Cyclin-dependent kinase 9 is required for tumor necrosis factor-α-stimulated matrix metalloproteinase-9 expression in human lung adenocarcinoma Cells. *J. Biol. Chem.* **2005**, *280*, 1103−1111.
(29) Havlicek, L.; Fuksova, K.; Krystof, V.; Orsag, M.; Vojtesek, B.; Strnad, M. 8-Azapurines as new inhibitors of cyclin-dependent kinases. *Bioorg. Med. Chem.* **2005**, *13*, 5399−5407.
(30) Havlicek, L.; Hanus, J.; Vesely, J.; Leclerc, S.; Meijer, L.; Shaw, G.; Strnad, M. Cytokinin-derived cyclin-dependent kinase inhibitors: synthesis and cdc2 inhibitory activity of olomoucine and related compounds. *J. Med. Chem.* **1997**, *40*, 408−412.
(31) Krystof, V.; Lenobel, R.; Havlicek, L.; Kuzma, M.; Strnad, M. Synthesis and biological activity of olomoucine II. *Bioorg. Med. Chem. Lett.* **2002**, *12*, 3283−3286.
(32) Krystof, V.; McNae, I. W.; Walkinshaw, M. D.; Fischer, P. M.; Muller, P.; Vojtesek, B.; Orság, M.; Havlicek, L.; Strnad, M. Antiproliferative activity of olomoucine II, a novel 2,6,9-trisubstituted purine cyclin-dependent kinase inhibitor. *Cell. Mol. Life Sci.* **2005**, *62*, 1763−1771.
(33) Moravcova, D.; Krystof, V.; Havlicek, L.; Moravec, J.; Lenobel, R.; Strnad, M. Pyrazolo[4,3-d]pyrimidines as new generation of cyclin-dependent kinase inhibitors. *Bioorg. Med. Chem. Lett.* **2003**, *13*, 2989−2992.
(34) Moravec, J.; Krystof, V.; Hanus, J.; Havlicek, L.; Moravcova, D.; Fuksova, K.; Kuzma, M.; Lenobel, R.; Otyepka, M.; Strnad, M. 2,6,8,9-Tetrasubstituted Purines as New CDK1 Inhibitors. *Bioorg. Med. Chem. Lett.* **2003**, *13*, 2993−2996.
(35) Pevarello, P.; Brasca, M. G.; Amici, R.; Orsini, P.; Traquandi, G.; Corti, L.; Piutti, C.; Sansonna, P.; Villa, M.; Pierce, B. S.; Pulici, M.; Giordano, P.; Martina, K.; Fritzen, E. L.; Nugent, R. A.; Casale, E.; Cameron, A.; Ciomei, M.; Roletto, F.; Isacchi, A.; Fogliatto, G.; Pesenti, E.; Pastori, W.; Marsiglio, A.; Leach, K. L.; Clare, P. M.; Fiorentini, F.; Varasi, M.; Vulpetti, A.; Warpehoski, M. A. 3-Aminopyrazole inhibitors of CDK2/Cyclin A as antitumor agents. 1. Lead finding. *J. Med. Chem.* **2004**, *47*, 3367−3380.
(36) Pevarello, P.; Brasca, M. G.; Orsini, P.; Traquandi, G.; Longo, A.; Nesi, M.; Orzi, F.; Piutti, C.; Sansonna, P.; Varasi, M.; Cameron, A.; Vulpetti, A.; Roletto, F.; Alzani, R.; Ciomei, M.; Albanese, C.; Pastori, W.; Marsiglio, A.; Pesenti, E.; Fiorentini, F.; Bischoff, J. R.; Mercurio, C. 3-Aminopyrazole Inhibitors of CDK2/Cyclin A as antitumor agents. 2. Lead optimization. *J. Med. Chem.* **2005**, *48*, 2944−2956.
(37) Knockaert, M.; Gray, N.; Damiens, E.; Chang, Y.-T.; Grellier, P.; Grant, K.; Fergusson, D.; Mottram, J.; Soete, M.; Dubremetz, J.-F.; Le Roch, K.; Doerig, C.; Schultz, P. G.; Meijer, L. Intracellular targets of cyclin-dependent kinase inhibitors: identification by affinity chromatography using immobilised inhibitors. *Chem. Biol.* **2000**, *7*, 411−422.
(38) McClue, S. J.; Blake, D.; Clarke, R.; Cowan, A.; Cummings, L.; Fischer, P. M.; MacKenzie, M.; Melville, J.; Stewart, K.; Wang, S.; Zhelev, N.; Zheleva, D.; Lane, D. P. In vitro and in vivo antitumor properties of the cyclin dependent kinase inhibitor CYC202 (R-roscovitine). *Int. J. Cancer* **2002**, *102*, 463−468.

(39) Bain, J.; McLauchlan, H.; Elliott, M.; Cohen, P. The specificities of protein kinase inhibitors: an update. *Biochem. J.* **2003**, *371*, 199−204.
(40) Mettey, Y.; Gompel, M.; Thomas, V.; Garnier, M.; Leost, M.; Ceballos-Picot, I.; Noble, M.; Endicott, J.; Vierfond, J.-M.; Meijer, L. Aloisines, a new family of CDK/GSK-3 inhibitors. SAR study, crystal structure in complex with CDK2, enzyme selectivity, and cellular effects. *J. Med. Chem.* **2003**, *46*, 222−236.
(41) Zandomeni, R.; Zandomeni, M. C.; Shugar, D.; Weinmann, R. Casein kinase type II is involved in the inhibition by 5,6-dichloro-1-beta-D-ribofuranosylbenzimidazole of specific RNA polymerase II transcription. *J. Biol. Chem.* **1986**, *261*, 3414−3419.
(42) Meggio, F.; Shugar, D.; Pinna, L. A. Ribofuranosyl-benzimidazole derivatives as inhibitors of casein kinase-2 and casein kinase-1. *Eur. J. Biochem.* **1990**, *187*, 89−94.
(43) Wu, S. Y.; McNae, I.; Kontopidis, G.; McClue, S. J.; McInnes, C.; Stewart, K. J.; Wang, S.; Zheleva, D. I.; Marriage, H.; Lane, D. P.; Taylor, P.; Fischer, P. M.; Walkinshaw, M. D. Discovery of a novel family of CDK inhibitors with the program LIDAEUS: Structural basis for ligand-induced disordering of the activation loop. *Structure* **2003**, *11*, 399−410.
(44) Stepanic, V.; Baranovic, G.; Smrecki, V. Structure and vibrational spectra of conjugated acids of trans- and cis-azobenzene. *J. Mol. Struct.* **2001**, *569*, 89−109.
(45) De Azevedo, W. F., Jr.; Canduri, F.; Da Silveira, N. J. F. Structural basis for inhibition of cyclin-dependent kinase 9 by flavopiridol. *Biochem. Biophys. Res. Commun.* **2002**, *293*, 566−571.
(46) Vesely, J.; Havlicek, L.; Strnad, M.; Blow, J. J.; Donella-Deana, A.; Pinna, L.; Letham, D. S.; Kato, J.; Detivaud, L.; Leclerc, S.; Meijer, L. Inhibition of cyclin-dependent kinases by purine analogues. *Eur. J. Biochem.* **1994**, *224*, 771−786.
(47) Sherr, C. J. Principles of tumor suppression. *Cell* **2004**, *116*, 235−246.
(48) Kotala, V.; Uldrijan, S.; Horky, M.; Trbusek, M.; Strnad, M.; Vojtesek, B. Potent induction of wild-type p53-dependent transcription in tumour cells by a synthetic inhibitor of cyclin-dependent kinases. *Cell. Mol. Life Sci.* **2001**, *58*, 1333−1339.
(49) Wang, S.; Meades, C.; Wood, G.; Osnowski, A.; Anderson, S.; Yuill, R.; Thomas, M.; Mezna, M.; Jackson, W.; Midgley, C.; Griffiths, G.; Fleming, I.; Green, S.; McNae, I.; Wu, S. Y.; McInnes, C.; Zheleva, D.; Walkinshaw, M. D.; Fischer, P. M. 2-Anilino-4-(thiazol-5-yl)pyrimidine CDK inhibitors: Synthesis, SAR analysis, X-ray crystallography, and biological activity. *J. Med. Chem.* **2004**, *47*, 1662−1675.
(50) Kontopidis, G.; Andrews, M. J. I.; McInnes, C.; Cowan, A.; Powers, H.; Innes, L.; Plater, A.; Griffiths, G.; Paterson, D.; Zheleva, D. I.; Lane, D. P.; Green, S.; Walkinshaw, M. D.; Fischer, P. M. Insights into cyclin groove recognition: complex crystal structures and inhibitor design through ligand exchange. *Structure* **2003**, *11*, 1537−1546.
(51) Pflugrath, J. The finer things in X-ray diffraction data collection. *Acta Crystallogr.* **1999**, *D55*, 1718−1725.
(52) Murshudov, G. N.; Vagin, A. A.; Dodson, E. J. Refinement of macromolecular structures by the maximum-likelihood method. *Acta Crystallogr.* **1997**, *D53*, 240−255.
(53) Lamzin, V. S.; Wilson, K. S. Automated refinement for protein crystallography. *Methods Enzymol.* **1997**, *277*, 269−305.
(54) Uchoa, H. B.; Jorge, G. E.; Freitas Da Silveira, N. J.; Camera, J. C., Jr.; Canduri, F.; De Azevedo, W. F., Jr. Parmodel: a web server for automated comparative modeling of proteins. *Biochem. Biophys. Res. Commun.* **2004**, *325*, 1481−1486.

JM0605740